

Journal of Materials Chemistry A

Accepted Manuscript



This is an *Accepted Manuscript*, which has been through the Royal Society of Chemistry peer review process and has been accepted for publication.

Accepted Manuscripts are published online shortly after acceptance, before technical editing, formatting and proof reading. Using this free service, authors can make their results available to the community, in citable form, before we publish the edited article. We will replace this *Accepted Manuscript* with the edited and formatted *Advance Article* as soon as it is available.

You can find more information about *Accepted Manuscripts* in the [Information for Authors](#).

Please note that technical editing may introduce minor changes to the text and/or graphics, which may alter content. The journal's standard [Terms & Conditions](#) and the [Ethical guidelines](#) still apply. In no event shall the Royal Society of Chemistry be held responsible for any errors or omissions in this *Accepted Manuscript* or any consequences arising from the use of any information it contains.



www.rsc.org/materialsA

Cite this: DOI: 10.1039/c0xx00000x

www.rsc.org/xxxxxx

ARTICLE TYPE

MoS₂ nanosheets-coated CoS₂ nanowire arrays on carbon cloth as three-dimensional electrodes for efficient electrocatalytic hydrogen evolution†

Jilin Huang^a, Dongman Hou^b, Yucheng Zhou^a, Weijia Zhou^{a*}, Guoqiang Li^b, Zhenghua Tang^a, Ligui Li^a, and Shaowei Chen^{a,c*}

Received (in XXX, XXX) Xth XXXXXXXXX 20XX, Accepted Xth XXXXXXXXX 20XX

DOI: 10.1039/b000000x

Design and engineering of low-cost and high-efficiency electrocatalysts for hydrogen evolution reaction (HER) has attracted increasing interest in renewable energy research. Herein, MoS₂ nanosheets-coated CoS₂ nanowire arrays supported on carbon cloth (MoS₂/CoS₂/CC) were prepared by a two-step procedure that entailed hydrothermal growth of Co(OH)₂ nanowire arrays on carbon cloth, followed by reaction with (NH₄)₂MoS₄ to grow an overlayer of MoS₂ nanosheets. Electrochemical studies showed that the obtained 3D electrode exhibited excellent HER activity with an overpotential of -87 mV at 10 mA cm⁻², a small Tafel slope of 73.4 mV dec⁻¹ and prominent electrochemical durability. The results presented herein may offer a new methodology for the design and engineering of effective multilevel structured catalysts for HER based on earth-abundant components.

Introduction

Hydrogen has been hailed as a sustainable, secure, and clean alternative energy source that may satisfy the growing global energy demand. Yet such a promise will be realized only when the production of hydrogen can be carried out in an efficient, low-cost, and environmentally friendly fashion. Electrocatalytic hydrogen evolution reaction (HER) is a highly attractive means for meeting these requirements.¹⁻³ Among the various HER electrocatalysts, noble metals such as Pt have been the catalysts of choice thus far, but scarcity and high costs have severely limited their practical applicability.⁴⁻⁷ In recent years, a great deal of research efforts have been directed to using earth abundant and inexpensive materials to replace Pt as HER electrocatalysts, including transition metal sulfides,^{1, 7-11} selenides¹² carbides,¹³⁻¹⁵ and phosphides.¹⁶⁻²⁰ Among these, MoS₂ has received particular attention due to the earth-abundant composition and high activity.²¹⁻²⁸ Yet, with the anisotropic structure of the sandwiched S-Mo-S layers, MoS₂ is prone to form a two-dimensional (2D) morphology leading to a limited number of active sites for HER.

The catalytic performance may be further improved by doping other atoms into the catalysts by manipulation of the hydrogen adsorption energy. In fact, a variety of transition metal or non-metal atoms have been used as dopants, such as Co, Ni, Li, N, Cl and O.^{21, 29-34} For example, the Dai group reported the synthesis of highly active and stable hybrid electrocatalysts for HER based on Co-doped iron pyrite (FeS₂) supported on carbon nanotubes (Fe_{1-x}Co_xS₂/CNT), which achieved a low overpotential of -0.12 V at 20 mA cm⁻², a Tafel slope of 46 mV dec⁻¹, and excellent stability over 40 h in acid solution.³⁵ Xie and coworkers demonstrated the synergistic

regulation of both structural and electronic benefits from controllable disorder engineering and simultaneous O atoms incorporation into MoS₂, and observed dramatically enhanced HER activity.³⁰

Moreover, with increasing roughness of the electrode, one anticipates to see a decrease of the electrode size and an increase of the number of catalytic sites available for HER. Within this context, nanowires arrays integrated with a conducting substrate may enjoy the additional advantages of both charge carrier transport and the release of evolved hydrogen gas from the electrode surface.³⁶⁻³⁸ Note that cobalt pyrite (CoS₂) has been reported to be catalytically active for HER with metal-like conductivity.³⁹ Therefore, CoS₂ nanowire arrays may be an ideal three-dimensional (3D) conductive substrate that features high HER activity.

In order to meet the above requirements (high electrochemical active area, high conductivity and abundant catalytic active sites), we designed and synthesized an HER electrode based on a hybrid structure consisting of CoS₂ nanowires coated with cobalt and oxygen co-doped MoS₂ nanosheets on carbon cloth (MoS₂/CoS₂/CC). The resulting nanocomposites exhibited remarkable HER stability and activity. Experimentally, CoS₂ nanowires arrays were used as 3D electrodes to obtain a high electrochemically active surface area. Cobalt and oxygen co-doped MoS₂ nanosheets were then concurrently grown on the CoS₂ nanowire surface. The obtained MoS₂/CoS₂ hybrids exhibited a low overpotential of only -87 mV at 10 mA cm⁻², a small Tafel slope of 73.4 mV dec⁻¹, and good catalytic stability.

Experimental section

Chemicals. All reagents were of analytical grade and used

without further purification. Ammonium tetrathiomolybdate ((NH₄)₂MoS₄), sodium sulfide (Na₂S), cobalt chloride (CoCl₂·6H₂O), ammonium chloride (NH₄Cl), carbamide (CO(NH₂)₂), 20 wt% Pt/C, and carbon cloth (CC) were obtained from Sinopharm Chemical Reagents Beijing Co. and used as received. Water was supplied with a Barnstead Nanopure Water System (18.3 MΩ·cm).

Synthesis of Co(OH)₂ nanowires supported on CC. In a typical reaction, 0.29 g of CoCl₂·6H₂O, 0.92 g of NH₄Cl, and 0.37 g of CO(NH₂)₂ were dissolved in 20 mL of Nanopure water under vigorous stirring for 30 min. Then the solution was transferred into a Teflon-lined stainless autoclave (25 mL) and a piece of CC (3.5 cm × 2.2 cm; which was cleaned by ultrasonication in acetone, ethanol and water for 20 min each prior to use). The autoclave was sealed and heated at 120 °C for 6 h in an electric oven, and then air-cooled to room temperature. The carbon cloth was taken out and washed with water before being dried at 70 °C for 6 h, affording Co(OH)₂ nanowires supported on CC which were denoted as Co(OH)₂/CC.

Synthesis of MoS₂/CoS₂ heterostructures on carbon cloth (MoS₂/CoS₂/CC). Experimentally, 50 mg of (NH₄)₂MoS₄ was dissolved in 20 mL of Nanopure water to form a solution. Then the solution was transferred into a Teflon-lined stainless autoclave (25 mL) and a piece of Co(OH)₂/CC prepared above (2 cm × 0.5 cm) was immersed into the solution. The autoclave was heated at 200 °C for 24 h. The resulting MoS₂/CoS₂/CC (at a loading of about 18.6 mg cm⁻²) was harvested after being washed with water thoroughly and vacuum dried.

CoS₂/CC (at a loading of about 16.5 mg cm⁻²) was synthesized in a similar fashion but by using 50 mg of Na₂S instead of (NH₄)₂MoS₄. Another sample, MoS₂/CC (at a loading of about 4.2 mg cm⁻²), was prepared also by the same procedure where pristine CC (2 cm × 0.5 cm) was used instead of CoS₂/CC.

Characterizations. Scanning electron microscopic (SEM) analysis was carried out with a FEI NOVA NanoSEM 430 field-emission microscope. Transmission electron microscopic (TEM) measurements were carried out with a JOEL JEM 2100F microscope. Powder X-ray diffraction (XRD) patterns of the samples were recorded on a Bruke D8 Advance powder X-ray diffractometer with Cu Kα (λ = 0.15406 nm) radiation. X-ray photoelectron spectroscopic (XPS) measurements were performed using a PHI X-tool instrument (Ulvac-Phi). Raman spectra were recorded on a RENISHAW inVia instrument with an Ar laser source of 488 nm in a macroscopic configuration.

Electrochemistry. Electrochemical measurements were performed with an electrochemical workstation (CHI 760C, CH Instruments Inc.) in a 0.5 M H₂SO₄ aqueous solution. A saturated calomel electrode (SCE, sat'd KCl) and platinum plate were used as the reference and counter electrode, respectively. The MoS₂/CoS₂/CC prepared above was used directly as a binder-free working electrode. The current densities were evaluated in terms of the geometrical surface area of MoS₂/CoS₂/CC. Polarization curves were acquired by sweeping the potential from 0 to -0.5 V (vs. RHE) at a potential sweep rate of 5 mV s⁻¹. Electrochemical impedance spectroscopy (EIS) was carried out with an amplitude of 10 mV

and frequency range from 100 kHz to 0.01 Hz. The main arc in each EIS spectrum was fitted using a simplified Randles equivalent circuit, which consisted of a solution resistance (R_s) in series with a parallel arrangement of a charge-transfer resistance (R_{ct}) and a constant phase element (CPE), and the fitting parameters were estimated through the application of the Levenberg-Marquardt minimization procedure. Cyclic voltammetry (CV) was used to probe the electrochemical double layer capacitance at nonfaradaic potentials as a means to estimate the effective electrode surface area. Accelerated stability tests were performed in 0.5 M H₂SO₄ at room temperature by potential cycling between 0 and -0.4 V (vs. RHE) at a sweep rate of 100 mV s⁻¹ for a given number of cycles. Current-time responses were monitored by chronoamperometric measurements. The hydrogen gas production rate was quantified by gas chromatographic measurements (GC-2060F, LuNan Analytical Instruments, LTD, China).

Results and discussion

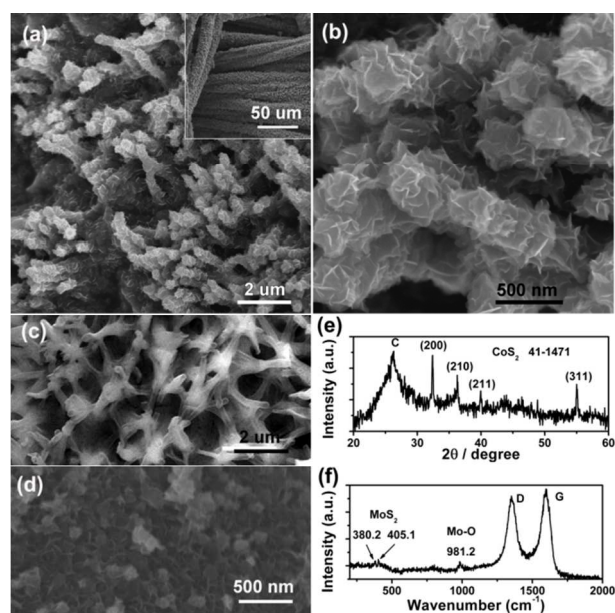


Figure 1. SEM images of (a, b) MoS₂/CoS₂/CC, (c) CoS₂/CC and (d) MoS₂/CC. (e) XRD patterns and (f) Raman spectrum of MoS₂/CoS₂/CC. Inset to Figure 1a is an SEM image of MoS₂/CoS₂/CC at low magnification.

Hierarchical MoS₂/CoS₂ arrays are synthesized by using Co(OH)₂ nanowires as a hard template (Figure S1). During the hydrothermal reaction, (NH₄)₂MoS₄ was decomposed into MoS₂ nanosheets and deposited on the surface of Co(OH)₂ nanowires. Concurrently, the redundant S ions released from (NH₄)₂MoS₄ reacted with Co(OH)₂ nanowires to form porous CoS₂ nanowires which served as structural backbones to guide the growth of MoS₂ nanosheets. SEM studies showed that the MoS₂/CoS₂ nanowires grew vertically and densely on CC (inset to Figure 1a) and the MoS₂/CoS₂ nanowires exhibited a diameter of ca. 500 nm and a length of 3 to 5 μm (Figure 1a). In fact, higher-magnification SEM measurements showed a uniform coverage of interconnected MoS₂ nanosheets on the

entire CoS₂ nanowires (Figure 1b). By contrast, CoS₂/CC exhibited only CoS₂ hollow nanotubes with diameters of about 500 nm (Figure 1c), and in MoS₂/CC only MoS₂ nanosheets can be seen (Figure 1d).

Figure 1e depicts the XRD patterns of MoS₂/CoS₂/CC. One can see four sharp peaks at $2\theta = 32.3, 36.2, 39.8$ and 55.1° which correspond to the (200), (210), (211), and (311) planes of CoS₂ (JCPDS no.41-1471). The broad diffraction peaks at $2\theta = 26.2^\circ$ arise from the CC substrate. No diffraction peak of MoS₂ can be detected, possibly due to a low content and a small thickness of only a few layers. However, Raman measurements (Figure 1f) of MoS₂/CoS₂/CC show two peaks at 380.2 and 405.1 cm^{-1} which are characteristic for MoS₂, confirming the formation of MoS₂. Note that the peak positions are similar to those of Li-doped 1T-MoS₂,²¹ possibly due to Co-doping or the formation of MoS₂/CoS₂ heterostructures. In addition, the vibrational band at 981.2 cm^{-1} suggested the formation of Mo-O bonds,^{21, 31} implying the doping of O into MoS₂ during the decomposition of Co(OH)₂. The peaks at 1350.4 and 1593.8 cm^{-1} are characteristic of the D and G vibrational bands of the graphitic CC substrate.

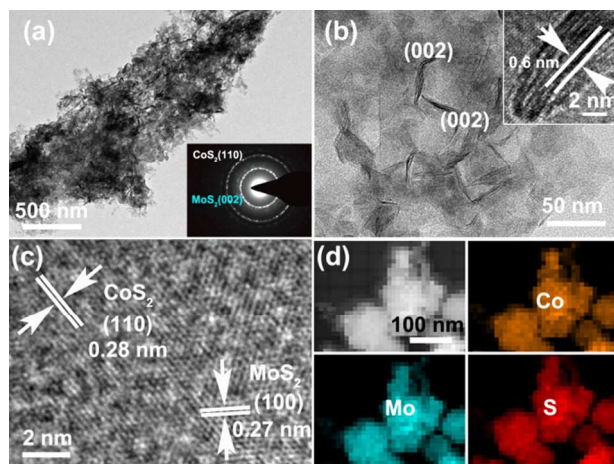


Figure 2. (a-c) Representative TEM images of MoS₂/CoS₂. Inset to Figure 2a is the selected area electron diffraction patterns of MoS₂/CoS₂; and inset to panel (b) is a high-resolution TEM image of MoS₂/CoS₂. (d) The corresponding EDX elemental mapping images of Mo, Co and S for MoS₂/CoS₂.

The structure and morphology of MoS₂/CoS₂ were further investigated by (HR)TEM measurements. Figure 2a shows a typical TEM image of an individual CoS₂ nanowire covered by thin MoS₂ nanosheets. The MoS₂ nanosheets were about 10 nm thick and grown tightly on the CoS₂ nanowire surface. It should be noted that the CoS₂ nanowires possessed a porous structure during the reaction between (NH₄)₂MoS₄ and Co(OH)₂. Thus, the interface between the CoS₂ backbone and the MoS₂ shell is difficult to identify. In the TEM image in Figure 2b, the layered structures of MoS₂ nanosheets can be clearly seen with an interlayer distance of 0.62 nm that is consistent with the MoS₂

(002) crystalline planes (inset to Figure 2b). In Figure 2c, one can see well-defined lattice fringes with a spacing of 0.27-0.28 nm, which is consistent with both CoS₂ (110) (0.28 nm) and MoS₂ (100) (0.27 nm). The coexistence of CoS₂ and MoS₂ was also manifested by the diffraction rings in the selected area electron diffraction (SAED) patterns (inset to Figure 2a). Notably, the similar interplanar spacing between CoS₂ (110) and MoS₂ (100) suggests good lattice matching, which might be beneficial in the formation of a strong heterogeneous structure.^{40,41} In fact, elemental mapping studies confirmed the intimate contact between CoS₂ and MoS₂ in MoS₂/CoS₂ with a homogeneous distribution of the S element (Figure 2d). Additionally, it revealed the co-existence of Co element within MoS₂, in spite of the relatively low content. This suggests the formation of Co-doped MoS₂.

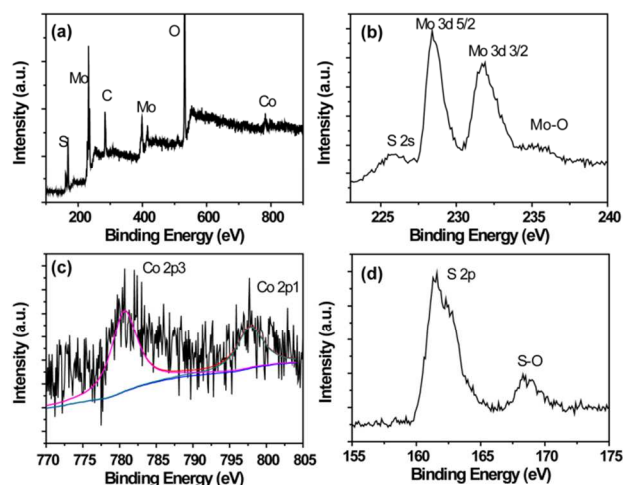


Figure 3. (a) XPS survey spectrum and high-resolution scans of (b) Mo 3d, (c) Co 2p and (d) S 2p electrons of MoS₂/CoS₂/CC. Black curves are experimental data and colored curves are deconvolution fits.

XPS measurements are then carried out to evaluate the chemical compositions as well as elemental valence states. The survey spectrum in Figure 3a confirms the presence of Co, Mo, S, C and O elements in MoS₂/CoS₂/CC. From the high-resolution scan in Figure 3b, the Mo 3d spectrum may be deconvoluted into two peaks at 228.3 and 231.8 eV. In addition, the characteristic peaks for Mo 3d in Mo-O and S2p in S-O bonds can be observed at 235.3 and 168.6 eV in Figure 3b and 3d, respectively, whereas the S 2p electrons in MoS₂ are manifested by the two peaks at 225.8 eV and 161.7 eV. These signify O-doping in MoS₂.^{42, 43} For the Co 2p electrons (Figure 3c), two distinct peaks can be identified at 780.9 and 797.6 eV, which can be assigned to Co 2p_{3/2} and Co 2p_{1/2}, respectively. Furthermore, based on the integrated peak areas of Co 2p and S-O, the atomic contents of Co and O in MoS₂ are estimated to be 0.8 and 4.9 at%, respectively.

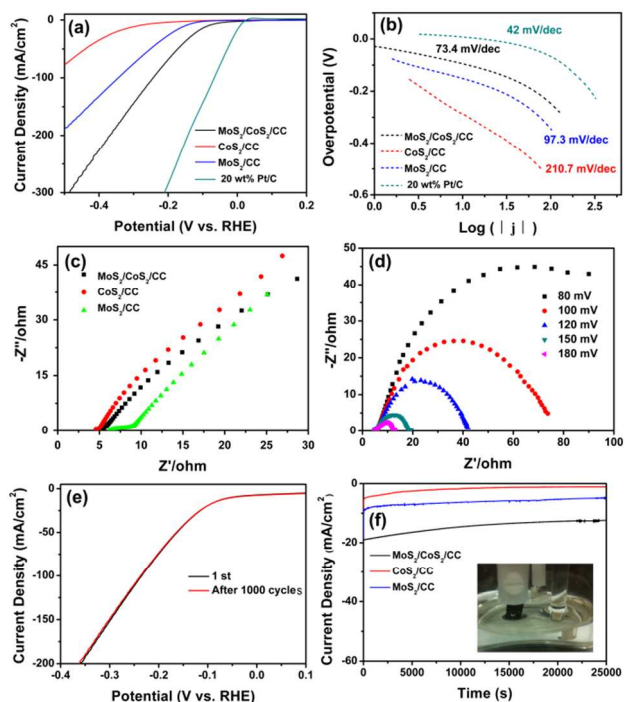


Figure 4. (a) Polarization curves for HER in 0.5 M H₂SO₄ at MoS₂/CoS₂/CC, CoS₂/CC, MoS₂/CC and 20 wt% Pt/C on CC. Potential sweep rate 5 mV s⁻¹. (b) Corresponding Tafel plots derived from (a). (c) Nyquist plots of MoS₂/CoS₂/CC, CoS₂/CC, and MoS₂/CC at open-circuit potentials. (d) Nyquist plots of MoS₂/CoS₂/CC at various HER overpotentials in 0.5 M H₂SO₄. (e) HER polarization curves for MoS₂/CoS₂/CC before and after 1,000 cycles in the stability test. (f) Current–time plots of the MoS₂/CoS₂/CC, CoS₂/CC and MoS₂/CC electrodes at the applied potential of –0.15 V (vs RHE). Inset shows the generation of hydrogen bubbles on the electrode surface.

Interestingly, the MoS₂/CoS₂/CC nanocomposites exhibited apparent HER activity in 0.5 M H₂SO₄. Experimentally, MoS₂/CoS₂/CC was used directly as an electrode without a binding agent or conducting additive. The iR-uncorrected polarization curves in Figure 4a show that the MoS₂/CoS₂/CC electrode exhibited a much better HER performance than CoS₂/CC and MoS₂/CC. For instance, At 10 mA cm⁻², the overpotential of MoS₂/CoS₂/CC was –87 mV, while higher than that of 20 wt% Pt/C (–4 mV), markedly smaller than those of CoS₂/CC (–288 mV) and MoS₂/CC (–155 mV). The enhanced HER activity of MoS₂/CoS₂/CC might be ascribed to the synergistic effects between CoS₂ and MoS₂.

The Tafel slopes of the various samples were then analyzed and compared (Figure 4b), by fitting the linear portions of the polarization curves with the Tafel equation ($\eta = \text{blog } j + a$), where j is the current density and b is the Tafel slope. The Tafel slope of MoS₂/CoS₂/CC is estimated to be 73.4 mV dec⁻¹, which is drastically lower than those of other samples, for example, MoS₂/CC (97.3 mV dec⁻¹) and CoS₂/CC (210.7 mV dec⁻¹), but higher than that of the 20 wt% Pt/C (42 mV dec⁻¹). A lower Tafel slope typically corresponds to more favorable HER kinetics, further confirming the synergistic contribution of the CoS₂ and MoS₂. EIS measurements were then carried out to further probe the electron-transfer kinetics involved. As shown in the Nyquist plots (Figure 4c), the solution resistance (R_s) for

MoS₂/CoS₂/CC is small, less than 5.2 Ω, close to that of CoS₂/CC (4.5 Ω), but lower than that of MoS₂/CC (6.3 Ω). The results confirm that CoS₂ possessed high conductivity due to the metal-like conductivity property. Additionally, the charge transfer resistance (R_{ct}) diminished markedly with increasing overpotential from 126 Ω at –80 mV to 4.3 Ω at –180 mV, suggesting enhanced electron-transfer kinetics with increasing overpotentials, as depicted in Figure 4d.

In addition to excellent catalytic activity, MoS₂/CoS₂/CC also exhibited extraordinary stability in acid solution. Figure 4e depicts the polarization curves of MoS₂/CoS₂/CC before and after the stability tests of 1,000 potential cycles, where the current remained virtually unchanged. Moreover, after 25,000 s' continuous operation at the applied potential of –0.15 V (vs. RHE), the current density of MoS₂/CoS₂/CC remained virtually invariant, once again confirming the remarkable HER stability in 0.5 M H₂SO₄ solution (Figure 4f). In addition, one can see that the current density of the MoS₂/CoS₂/CC electrode was markedly larger than those of CoS₂/CC and MoS₂/CC at the same applied potential. The generation of hydrogen was confirmed by GC analysis (and manifested by the generation of hydrogen bubbles on the electrode surface, as depicted in Figure 4f inset), which was quantitatively consistent with those estimated from i-t data (Figure S2). The Faradaic efficiency (FE) was calculated by comparing the amount of experimentally quantified hydrogen with the theoretical value, which was 89.3% for CoS₂/CC, 100% for MoS₂/CC, and 96.8% for MoS₂/CoS₂/CC. This suggests that MoS₂ can improve the catalytic stability of CoS₂. After i-t testing, the morphologies of MoS₂/CoS₂/CC displayed no apparent changes, which confirmed the strong structural stability of the hybrid electrodes (Figure S3).

It should be noted that such an HER performance of MoS₂/CoS₂/CC (–87 mV vs. RHE at 10 mA cm⁻², Tafel slope of 73.4 mV dec⁻¹, and excellent catalytic stability) is better than or at least comparable to those of the MoS₂ or CoS₂-based HER electrocatalysts in acidic solution (Table S1), for instance, metallic CoS₂ nanostructures (–148 mV vs. RHE at 10 mA cm⁻², and Tafel slope of 51.6 mV dec⁻¹),³⁹ metallic CoS₂ nanopyramid arrays (–67 mV vs. RHE at 10 mA cm⁻², and Tafel slope of 70.1 mV dec⁻¹),⁴⁴ Li-doped MoS₂/CC (–118 mV vs. RHE at 10 mA cm⁻², iR-corrected, and Tafel slope of 62 mV dec⁻¹),³³ N-doped carbon-coated cobalt nanorod arrays on a Titanium mesh (–106 mV vs. RHE at 10 mA cm⁻², and Tafel slope of 78.2 mV dec⁻¹),³⁶ etc.

The remarkable HER performance of the MoS₂/CoS₂ hierarchical arrays observed above might be rationalized as follows: (1) the high conductivity of the CC substrate and the metal-like CoS₂ facilitated electron transport during hydrogen evolution; (2) the 3D hierarchical structure of the MoS₂/CoS₂ arrays exhibited a high electrochemically active surface area with abundant active sites (double-layer capacitance 7.04 mF cm⁻², Figure S4);⁴³ (3) doping by Co and O into MoS₂ produced abundant defect sites that served as catalytically active sites for HER, as suggested by Raman and HRTEM measurements (Figure 1f and Figure 2); and (4) synergetic interactions between CoS₂ and MoS₂ at the interface induced electron transfer between Co and Mo, leading to enhanced

electrocatalytic activity.⁴⁵

Conclusions

In this study, a nanocomposite based on MoS₂ nanosheets-coated CoS₂ nanowires arrays supported on carbon cloth (MoS₂/CoS₂/CC) were prepared by a two-step procedure that entailed hydrothermal growth of a Co(OH)₂ nanowire array on carbon cloth, followed by reaction with (NH₄)₂MoS₄ to obtain the MoS₂/CoS₂ composite structure. Electrochemical studies showed that the obtained 3D electrode exhibited excellent HER activity with an overpotential of -87 mV at 10 mA cm⁻², a small Tafel slope of 73.4 mV dec⁻¹ and prominent electrochemical durability. The high HER performance was mainly attributed to the synergistic effects of co-doping of Co and O into MoS₂ nanosheets and hence the formation of structural defects, good conductivity of metallic CoS₂, and high electrochemically active surface area of the hierarchical 3D structure. The results presented herein may offer a new methodology for the design and engineering of effective HER catalysts based on earth-abundant and inexpensive components.

Acknowledgements

This work was supported by the National Recruitment Program of Global Experts, Zhujiang New Stars of Science & Technology (2014J2200061), Project of Public Interest Research and Capacity Building of Guangdong Province (2014A010106005), the Fundamental Research Funds for the Central Universities, the National Natural Science Foundation of China (51502096), the National Science Fund for Excellent Young Scholars of China (51422203), and Excellent Youth Foundation of Guangdong Scientific Committee (S2013050013882).

Notes and references

^a New Energy Research Institute, School of Environment and Energy, South China University of Technology, Guangzhou Higher Education Mega Center, Guangzhou, Guangdong 510006, China; E-mail: eszhouwj@scut.edu.cn

^b State Key Laboratory of Luminescent Materials and Devices, South China University of Technology, 381 Wushan Road, Guangzhou 510641, China

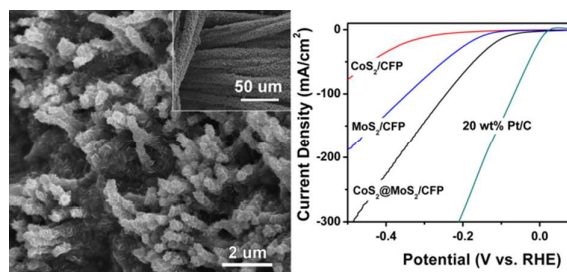
^c Department of Chemistry and Biochemistry, University of California, 1156 High Street, Santa Cruz, California 95064, United States; E-mail: Shaowei@ucsc.edu

† Electronic Supplementary Information (ESI) available: Additional experimental data and discussion, Figures S1-S4. See DOI: 10.1039/b000000x/

- J. Yang and H. S. Shin, *J Mater Chem A*, 2014, 2, 5979-5985.
- J. R. McKone, N. S. Lewis and H. B. Gray, *Chem Mater*, 2014, 26, 407-414.
- J. Luo, J.-H. Im, M. T. Mayer, M. Schreier, M. K. Nazeeruddin, N.-G. Park, S. D. Tilley, H. J. Fan and M. Grätzel, *Science*, 2014, 345, 1593-1596.
- S. Bai, C. Wang, M. Deng, M. Gong, Y. Bai, J. Jiang and Y. Xiong, *Angew Chem Int Ed*, 2014, 53, 12120-12124.
- R. Subbaraman, D. Tripkovic, D. Strmcnik, K.-C. Chang, M. Uchimura, A. P. Paulikas, V. Stamenkovic and N. M. Markovic, *Science*, 2011, 334, 1256-1260.
- I. E. L. Stephens and I. Chorkendorff, *Angew Chem Int Ed*, 2011, 50, 1476-1477.
- D. Hou, W. Zhou, X. Liu, K. Zhou, J. Xie, G. Li and S. Chen, *Electrochim Acta*, 2015, 166, 26-31.
- S. Peng, L. Li, X. Han, W. Sun, M. Srinivasan, S. G. Mhaisalkar, F. Cheng, Q. Yan, J. Chen and S. Ramakrishna, *Angew Chem Int Ed*, 2014, 53, 12594-12599.
- Y. Yang, H. Fei, G. Ruan, C. Xiang and J. M. Tour, *Adv Mater*, 2014, 26, 8163-8168.
- M. S. Faber, M. A. Lukowski, Q. Ding, N. S. Kaiser and S. Jin, *The J Phys Chem C*, 2014, 118, 21347-21356.
- Y. Sun, C. Liu, D. C. Grauer, J. Yano, J. R. Long, P. Yang and C. J. Chang, *J Am Chem Soc*, 2013, 135, 17699-17702.
- D. Kong, H. Wang, Z. Lu and Y. Cui, *J Am Chem Soc*, 2014, 136, 4897-4900.
- X. Fan, H. Zhou and X. Guo, *ACS Nano*, 2015, 9, 5125-5134.
- L. Liao, S. Wang, J. Xiao, X. Bian, Y. Zhang, M. D. Scanlon, X. Hu, Y. Tang, B. Liu and H. H. Girault, *Energy Environ Sci*, 2014, 7, 387-392.
- H. B. Wu, B. Y. Xia, L. Yu, X.-Y. Yu and X. W. Lou, *Nat Commun*, 2015, 6.
- E. J. Popczun, J. R. McKone, C. G. Read, A. J. Biacchi, A. M. Wiltrout, N. S. Lewis and R. E. Schaak, *J Am Chem Soc*, 2013, 135, 9267-9270.
- Z. Xing, Q. Liu, A. M. Asiri and X. Sun, *Adv Mater*, 2014, 26, 5702-5707.
- S. Gu, H. Du, A. M. Asiri, X. Sun and C. M. Li, *Phys Chem Chem Phys*, 2014, 16, 16909-16913.
- P. Jiang, Q. Liu, C. Ge, W. Cui, Z. Pu, A. M. Asiri and X. Sun, *J Mater Chem A*, 2014, 2, 14634-14640.
- Q. Liu, J. Tian, W. Cui, P. Jiang, N. Cheng, A. M. Asiri and X. Sun, *Angew Chem Int Ed*, 2014, 126, 6828-6832.
- M. A. Lukowski, A. S. Daniel, F. Meng, A. Forticaux, L. Li and S. Jin, *J Am Chem Soc*, 2013, 135, 10274-10277.
- D. Voiry, M. Salehi, R. Silva, T. Fujita, M. Chen, T. Asefa, V. B. Shenoy, G. Eda and M. Chhowalla, *Nano Lett*, 2013, 13, 6222-6227.
- J. Duan, S. Chen, M. Jaroniec and S. Z. Qiao, *ACS Nano*, 2015, 9, 931-940.
- L. Yang, W. Zhou, D. Hou, K. Zhou, G. Li, Z. Tang, L. Li and S. Chen, *Nanoscale*, 2015, 7, 5203-5208.
- S. Chen, J. Duan, Y. Tang, B. Jin and S. Zhang Qiao, *Nano Energy*, 2015, 11, 11-18.
- D. Merki, S. Fierro, H. Vrubel and X. Hu, *Chem Sci*, 2011, 2, 1262-1267.
- H. Wang, Z. Lu, S. Xu, D. Kong, J. J. Cha, G. Zheng, P.-C. Hsu, K. Yan, D. Bradshaw and F. B. Prinz, *Proc Nat Acad Sci*, 2013, 110, 19701-19706.
- J. D. Benck, Z. Chen, L. Y. Kuritzky, A. J. Forman and T. F. Jaramillo, *ACS Catal*, 2012, 2, 1916-1923.
- D. Merki, H. Vrubel, L. Rovelli, S. Fierro and X. Hu, *Chem Sci*, 2012, 3, 2515-2525.
- J. Xie, J. Zhang, S. Li, F. Grote, X. Zhang, H. Zhang, R. Wang, Y. Lei, B. Pan and Y. Xie, *J Am Chem Soc*, 2013, 135, 17881-17888.
- W. Zhou, D. Hou, Y. Sang, S. Yao, J. Zhou, G. Li, L. Li, H. Liu and S. Chen, *J Mater Chem A*, 2014, 2, 11358-11364.

-
32. W. J. Zhou, Y. H. Leng, D. M. Hou, H. D. Li, L. G. Li, G. Q. Li, H. Liu and S. W. Chen, *Nanoscale*, 2014, 6, 4698-4704.
33. H. Wang, Z. Lu, D. Kong, J. Sun, T. M. Hymel and Y. Cui, *ACS Nano*, 2014, 8, 4940-4947.
- 5 34. Q. Ding, F. Meng, C. R. English, M. Cabán-Acevedo, M. J. Shearer, D. Liang, A. S. Daniel, R. J. Hamers and S. Jin, *J Am Chem Soc*, 2014, 136, 8504-8507.
35. D.-Y. Wang, M. Gong, H.-L. Chou, C.-J. Pan, H.-A. Chen, Y. Wu, M.-C. Lin, M. Guan, J. Yang, C.-W. Chen, Y.-L. Wang, B.-J. Hwang, C.-C. Chen and H. Dai, *J Am Chem Soc*, 2015, 137, 1587-1592.
- 10 36. W. Zhou, Y. Zhou, L. Yang, J. Huang, Y. Ke, K. Zhou, L. Li and S. Chen, *J Mater Chem A*, 2015, 3, 1915-1919.
37. W. Zhou, X.-J. Wu, X. Cao, X. Huang, C. Tan, J. Tian, H. Liu, J. Wang and H. Zhang, *Energy Environ Sci*, 2013, 6, 2921-2924.
- 15 38. P. Jiang, Q. Liu, Y. Liang, J. Tian, A. M. Asiri and X. Sun, *Angew Chem Int Ed*, 2014, 53, 12855-12859.
39. M. S. Faber, R. Dziedzic, M. A. Lukowski, N. S. Kaiser, Q. Ding and S. Jin, *J Am Chem Soc*, 2014, 136, 10053-10061.
- 20 40. W. Zhou, H. Liu, J. Wang, D. Liu, G. Du and J. Cui, *ACS Appl Mater Interfaces*, 2010, 2, 2385-2392.
41. W. Zhou, Z. Yin, Y. Du, X. Huang, Z. Zeng, Z. Fan, H. Liu, J. Wang and H. Zhang, *Small*, 2013, 9, 140-147.
42. Z. Chen, D. Cummins, B. N. Reinecke, E. Clark, M. K. Sunkara and T. F. Jaramillo, *Nano Lett*, 2011, 11, 4168-4175.
- 25 43. X. Liu, W. Zhou, L. Yang, L. Li, Z. Zhang, Y. Ke and S. Chen, *J Mater Chem A*, 2015, 3, 8840-8846.
44. W. A. Bhutto, Z. Wu, Y. Cao, W. Wang, J. He, Q. Luo, S. Li, H. Li and J. Kang, *J Mater Chem A*, 2015, 3, 6360-6365.
- 30 45. H. Zhu, J. Zhang, R. Yanzhang, M. Du, Q. Wang, G. Gao, J. Wu, G. Wu, M. Zhang and B. Liu, *Adv Mater*, 2015.

ToC Graph



MoS₂ nanosheets-coated CoS₂ nanowires arrays supported on carbon cloth exhibited excellent HER activity with an overpotential of -87 mV (vs RHE) at 10 mA cm^{-2} due to the synergistic interactions between MoS₂ and CoS₂.